0.1 Introduction

0.1.1 Energy Dissipation rate from the tail spectrum

Most of the existing third generation wave prediction models (and WAVEWATCH III is no exception) have a cut-off frequency too small to represent some of the higher-frequency waves. To compensate this short-coming most wave models patch a "spectrum tail" to the spectrum resolved by the wave model. In the wave model setting we are using Donelan's spectrum tail Donelan (1987). This spectrum tail represents the wind-generated waves. For wind-generated gravity waves, Phillips (1985), showed that it exists a spectral equilibrium range where the source terms for the wind input (S_w), the non-linear interactions (S_{nl}) and the dissipation (S_d) are balanced.

$$S_w + S_{nl} + S_d = 0 \tag{1}$$

Because of the large uncertainties on the type of seas (swell, wind-wave or a mix of the two) considered beyond the peak frequency, we are considering that the equilibrium range is reached at the cut-off frequency of the WAVEWATCH III model. We are then only looking at the spectrum tail based on Donelan (1987). It assumes that, at the equilibrium range, the non-linear interactions are negligible compared to the other two terms. The balance is then just between S_w and S_d. The spectral rate of energy loss in the equilibrium range is given by :

$$\epsilon(k) = S_d(k) \tag{2}$$

where the dissipation is given by :

$$S_d(k) = \left[\omega\alpha\left(k^4\phi(k,\bar{\chi})\right)^n + \frac{4\nu k}{C}\right]\phi(k,\bar{\chi}) \tag{3}$$

where $\phi(k,\chi)$ is the tail spectrum given by :

$$\phi(k,\chi) = k^{-4}\left[\frac{0.28}{\alpha}\frac{\rho_a}{\rho_w}\left(\frac{\bar{U}cos(\chi-\bar{\chi})}{C} - 1\right)^2 - \frac{4\nu k}{\alpha C}\right]^{1/n} \tag{4}$$

where χ is the angle difference between the wind and the wave direction, $\bar{U}$ is the wind speed at half the wavelength height, ν is the kinematic water viscosity, α and n constants that varies as a function of k. As most of the

energy input and thus dissipation occurs when the waves and the wind are in the same direction, equation can be simplified as :

$$S_d(k) = \omega \left[0.28 \frac{\rho_a}{\rho_w} \left(\frac{\bar{U}}{C} - 1 \right)^2 \right] \phi(k, \bar{\chi}) \tag{5}$$

Based on equations (2) and (5) the energy dissipation rate is then a simple function of the wind speed and the wave number. Figure 1 shows the behavior of the energy dissipation rate as a function of k. You can notice that the curves for different wind speed start at different k because the cut-off frequency is different. The energy dissipation rates are larger at all wind speeds for the smaller wave numbers. As expected, the largest energy dissipation occurs at higher wind speed. However, as the wind speed increases the energy dissipation rates at lower wave numbers is less sensitive to the wind speed.

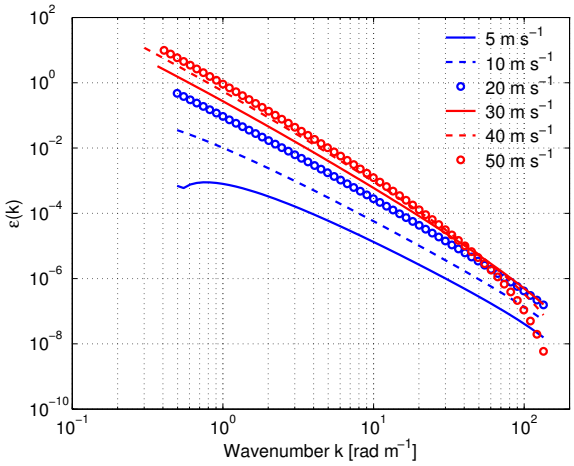

Figure 1: Energy Dissipation Rate for Different Wind Speed

By integrating the energy dissipation rate from the cut-off frequency wavenumber, k_{fcut} to higher frequencies, and multiplying by the water density (for dimensional purposes) the total rate of wave energy dissipation is :

$$\epsilon_t = \rho_w \int_{k_{fcut}} S_d(k) dk \tag{6}$$

The energy dissipation rate estimates obtained from the spectrum tail are well correlated with the wind speed (cf. fig.2a) but are not a linear function

of the wind speed. The peak winds for Hurricane Frances on 09/01 at 0600 UTC is 60 m s^{-1} in the right-front quadrant of the storm. The wind speed maximum is partially overlaying the energy dissipation maximum but the area covered by high energy dissipation rates expands beyond the location of the wind speed maximum area. Most of the energy dissipation occurs in the eyewall, particularly to the right of the storm where the winds are the strongest. The spectrum tail energy dissipation rates are fit by :

$$\epsilon_t = 1.277 \times 10^{-5} U^{3.2176} \tag{7}$$

Figure 2b shows the wind speed dependence of the energy dissipation rate for all the grid points for Hurricane Frances from 08/29 0000 UTC to 09/01 0600 UTC every 6-hourly. The tail presents two branches between 5 and 20 m s^{-1}. The major branch shows some significant scatter that increases with wind speed. The waves, when the storm is starting to intensify and at a latter stage are different. The energy dissipation increases for the same wind speed as the storm is maturing and the waves are more developed. Technically speaking, WAVEWATCH III is resolving the wave spectrum over a narrower wavenumber range. The tail patching is then starting at smaller wavenumbers. As shown earlier by figure 1 the energy dissipation is higher for lower wave number. So basically you are integrating over a larger range of wavenumbers but also higher energy dissipation rates.

The minor branch is coming from areas with shallower water depths. In these areas WAVEWATCH III is also somehow resolving the wave spectrum over a narrower range of wavenumbers. Those points in shallow waters represent only a small number of the total number of points considered to derive a relationship between the energy dissipation rates and the wind speed. However they exist and cannot be excluded.

Also, as shown by fig.2b, the dissipation estimates from Hanson and Phillips (1999) from the Gulf of Alaska show a similar wind speed dependence. There is however a nearly constant offset between the wind regression of the parametrized spectrum tail and the observational data. As explained in Hanson and Phillips (1999), this offset might be due to the difference in the atmospheric forcings. In their dataset obtained in the Gulf of Alaska during the winter, the wave field might be more developed than the wave fields in hurricane conditions. Furthermore, they were able to partition the wave spectrum in swell in wind sea and integrated the energy dissipation rate from the peak frequency of the wind sea to higher frequencies. In our case, we are considering only the wind sea from the tail, but there might

be some pure wind sea in the WAVEWATCH part of the spectrum. So the energy dissipation rates presented here might be an underestimate of the real energy dissipation.

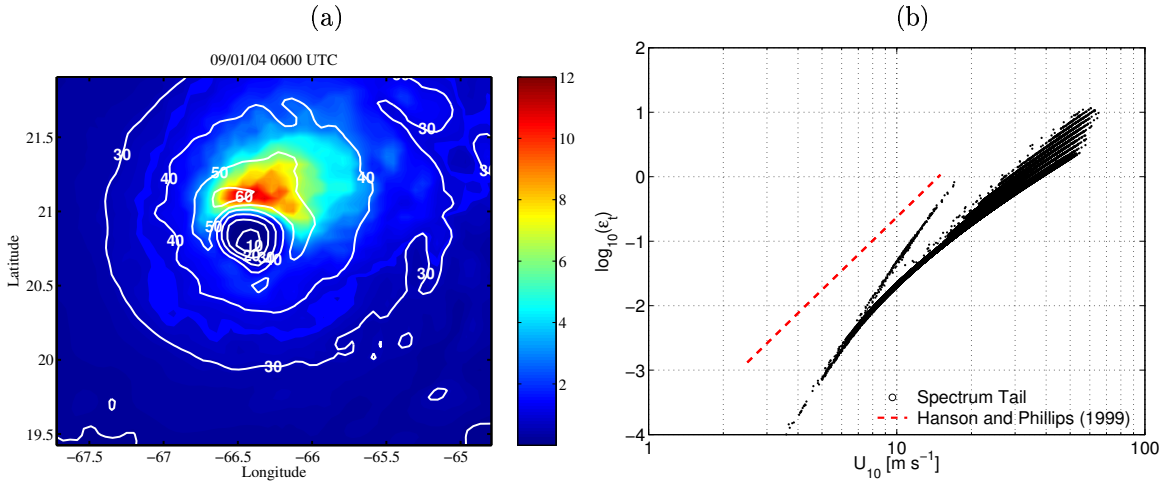

Figure 2: Energy Dissipation : a) for Hurricane Frances on 09/01 at 0600 UTC, b) as a function of wind speed (the dots represent the data from the spectrum tail for Hurricane Frances from 08/29 0000 UTC to 09/01 0600 UTC every 6-hourly and the dashed red line represents the data from Hanson and Phillips (1999)).

As explained earlier there is considerable spread of the energy dissipation at a later stage in the storm's lifetime than earlier (cf. fig.3a-b). For example, at 40 m s^{-1} the probability to have the energy dissipation to be around 1-1.5 kg s^{-3} is 66% if considering the values of energy dissipation rates from 08/29 0000 UTC to 08/29 at 0600 UTC (fig.3c). By incorporating 3 more days, the probability to have the energy dissipation around 1-1.5 kg s^{-3} is now 52% and there an increase in the probability to have higher energy dissipation rates (fig.3d). As there are only a few wind speeds beyond 60 m s^{-1},we do not attach any statistical significance to the values of energy dissipation beyond that point.

The energy dissipation is related to the white cap coverage. As the wave breaks it dissipates energy and one manifestation of the energy dissipation is the white capping at the sea surface. When the wave breaks, it generates two stages of white capping. The first response is the stage A (or active whitecap) (Monahan, 2001). When the wave initially breaks it produces

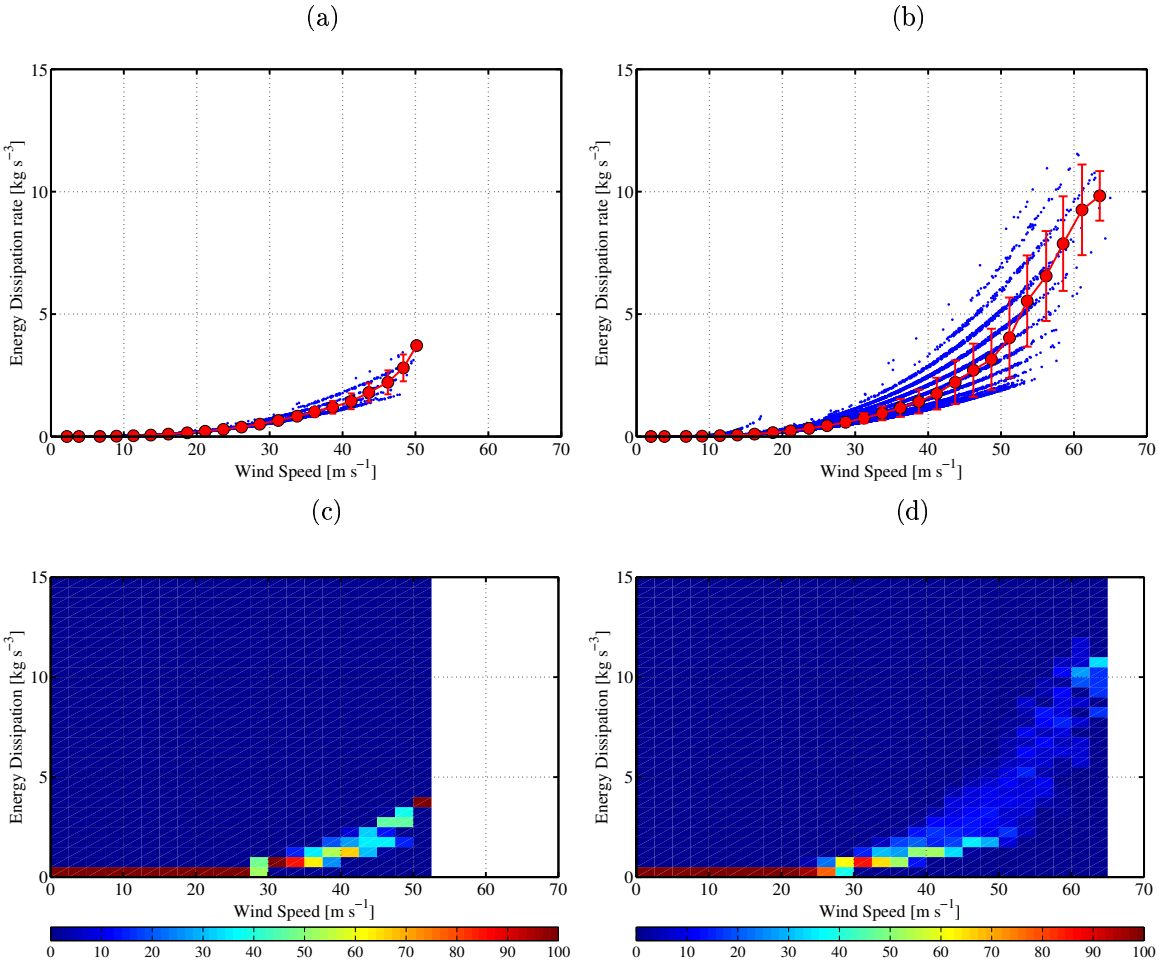

Figure 3: Energy Dissipation as a function of wind speed a) for 08/29/04 0600 UTC, b) for 09/01/04 0600 UTC (the red dots represent the mean value and the red vertical lines represent one standard deviation) and Probability Density Function (PDF) of Energy Dissipation as function of wind speed c) for 08/29/04 0600 UTC, d) for 09/01/04 0600 UTC

a cloud of bubbles (Monahan, 2001). The number of bubbles decreases with depth. They typically do not extend past a depth equivalent to the significant wave height (Monahan, 2001). The very white aspect of the sea surface and its high albedo during stage A, is a reflection of the large number of bubbles coming to the surface but also the large number of bubbles still present underneath it (Monahan, 2001). Stage B (or foam), is considered as the "daughter" of stage A (Monahan, 2001). It has a lower albedo as it is a decaying foam patch (Monahan, 2001). It usually covers an area ten times larger than stage A because of the intense turbulence generated during stage A Monahan (2001). The size difference between the stage A and B is enhanced in the presence of persistently spilling waves as the waves moves along the surface and leave a trail of whitecaps or in the presence of decaying patches within short distance of each other (Monahan, 2001). The concentration of bubbles during stage B is smaller than during stage A because most of the plume has been diffused over a greater area, the large bubbles occurred during stage A and the very small bubbles have been dissolved into the in the oceanic layer (Monahan, 2001).

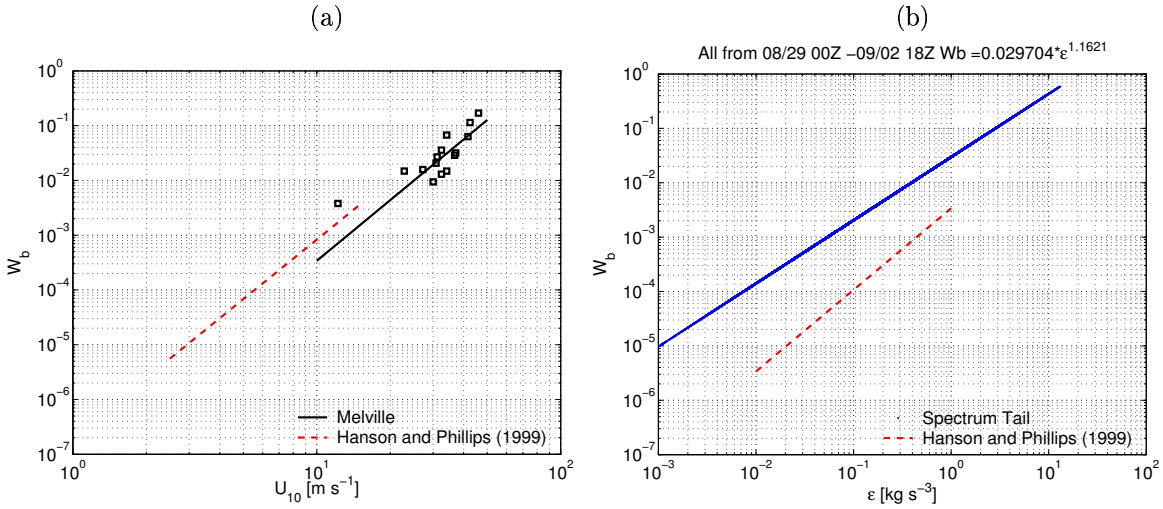

Figure 4: White cap fraction : a) as a function of wind speed, the black squares are the data from Melville in Hurricane Isabel 2003, the black line is a power fit trough those data, the red dashed line is the power fit from Hanson and Phillips (1999), b) as a function of the energy dissipation rate (the dots represent the data from the spectrum tail and the dashed red line represents the data from Hanson and Phillips (1999).

The white cap coverage as a function of wind speed is given by Melville for Hurricane Isabel. As pointed out by fig.4a the power fit trough Melville's data gives smaller values of white capping than Wu's fit (Wu, 1998). The white capping in Wu (1998) is representing the stage B white cap, which represents mostly the foam left behind after the initial breaking of the wave (stage A white cap). As explained in Monahan (2001), the area covered by the stage B white cap can be ten times the area covered during stage A. However, even when comparing the foam part (stage B) of Melville's data, the Wu's fit for the white cap is still an overestimate at every wind speed. The fit trough the Hanson and Phillips (1999) dataset (which is close to Wu's fit -1998-) shows higher white cap coverage for the same wind speed than the Melville's dataset. The Hanson and Phillips (1999) relationship between white cap and the wind speed (like the Wu's relationship) might be difficult to extrapolate to high wind speed. Around 60 m s^{-1}, the Hanson and Phillips (1999) fit shows a white cap coverage of 50 % and at 75 m s^{-1} shows more than a 100 % white cap coverage. By using Melville's fit for the white cap coverage eq. (8) and the fit from the spectrum tail given by eq. (7), we can deduce a relationship between the white cap coverage and the energy dissipation rate eq. (9).

$$W_b = 7.1101 \times 10^{-8} U^{3.68} \tag{8}$$

$$W_b = 2.8 \times 10^{-2} \epsilon^{1.1437} \tag{9}$$

The slopes of the two fits (spectrum tail and Hanson and Phillips (1999) dataset) are similar but with a nearly constant offset. The white cap coverage as a function of the energy dissipation rate obtained as a combination of the observed data in hurricane environment and the spectrum tail of the wave model show less energy dissipation for the same amount of white capping as shown by the Hanson and Phillips (1999) dataset from the Gulf of Alaska. There is almost an order of magnitude difference between the amount of energy dissipation rate necessary to produce the same amount of white capping between the two datasets.

Bibliography

Hanson, J. and O. M. Phillips, 1999: Wind sea growth and dissipation in the open ocean. *J. Phys. Oceanogr.*, **29**, 1633–1648.

Monahan, E. C., 2001: Whitecaps and foam. *Encyclopedia of Ocean Sciences*, Academic Press, J. Steele, S. Thorpe, and K. Turekian, eds., New York, 3213–3219.

Phillips, O. M., 1985: Spectral and statistical properties of the equilibrium range in wind-generated gravity waves. *J. Fluid Mech.*, **156**, 505–531.

Wu, J., 1998: Variations of whitecap coverage with wind stress and water temperature. *J. Phys. Oceanogr.*, **18**, 1448–1453.